Highly sensitive low power metal oxide sensors on nanoporous anodic alumina substrates

Gennady Gorokh, Igor Taratyn, Uladzimir Fiadosenka, Ilya Serdyuk, Linxi Dong, Chenxi Yue

Abstract—**The high physical, chemical, and mechanical properties of anodic alumina open up broad prospects for its use as a passive substrate for gas sensors. The results of practical tests of low-power thin-film gas microsensors manufactured on nanoporous anodic alumina substrates are presented. Due to the original design and the nanostructured gas-sensitive layers, the sensors had low power consumption and a high sensitivity to 10 ppm H_2 and 10 ppm CO. Comparative studies of gas sensor responses were carried out with three gas-sensitive layers of In_2O_3–Ga_2O_3; SnO_2–Pd and In_2O_3–SnO_2 at different operating temperatures. All sensors demonstrated high performance; in particular, the energy consumption during measurements did not exceed 30-40 mW, the maximum sensitivity for CO reached 350 %, and for H_2 up to 140 %, the response time was no more than 10 – 15 sec., and the regeneration time — no longer than 20 – 25 sec., high measurement reproducibility and operation stability, the drift of gas-sensitive layers was 3-5% over several months. With proper organization of production, such sensors are capable of competing with many advanced analogs**

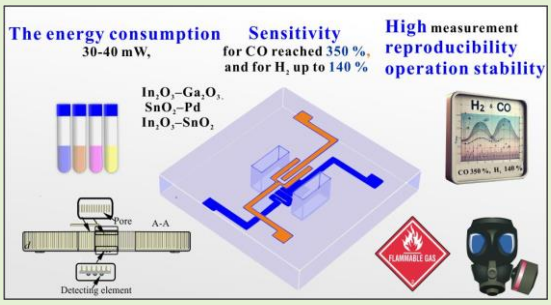

***Index Terms*—Semiconductor metal oxide composites; low power gas sensor; nanoporous anodic alumina substrates**

I. Introduction

In modern analytical equipment, a special place is occupied by semiconductor metal oxide gas sensors, the operating principle of which is based on the ability of gas-sensitive oxides to change their electrical characteristics through an adsorption-desorption process occurring on their surface when interacting with a gaseous environment [1-3]. The main analytical characteristics of gas metal oxide sensors are: *sensitivity* – detection limit for determining the minimum concentrations of the active gas; *selectivity* - the ability to distinguish one substance from others; *operating temperature range* - the temperature range in which the gas-sensitive layers provide maximum sensitivity; *response time* – the minimum time interval during which a change in the electrical conductivity of the active layer occurs; *regeneration time* – time for the sensor to return to its original state; *energy consumption* - energy expenditure required to heat the gas-sensitive layer to facilitate sorption processes. To improve the characteristics of sensors, special substrates and materials are used, new design solutions are used, and special technological methods and techniques are used. Most of these approaches are based on the production of sensors on silicon substrates using their micromechanical processing (MEMS technology) [4,5]. To increase the sensitivity of sensors, complex compositions of metal oxides and special methods of their application are used, which contribute to an increase in the specific surface area of the gas-sensitive layer [6,7]. To increase the selectivity of sensors when forming their sensitive layer, nanopowders and nanostructured films of metal oxides are used [8-10]. Often, an improvement in some parameters leads to a deterioration in others, for example, an increasing in the area of the gas-sensitive layer leads to an increase in thermal losses and a decrease in response time [11,12]. Compensation for this phenomenon led to an increase in the sensor power consumption. In practice, a solution was found that appeared capable of comprehensively solving this problem. The use of anodic alumina substrates (AAS) was proposed as the basis for the sensor [13–16]. The advantages of AAS include stable chemical and mechanical parameters such as elasticity, hardness, wear resistance [17–20], which allows the use of AAS in the design of gas sensors as a passive dielectric substrate to place structural elements. The unique structure of AAS, which is a regular ordered matrix of hexagonally packed oxide cells with cylindrical pores located in the center, makes it possible to nanostructure gas-sensitive films and multiply their active surface, and thereby increase the sensitivity and selectivity [21–23], and volumetric porosity has allowed significantly reducing thermal losses, which led to the decreasing in power consumption [24–26]. Furthermore, the nanostructured AAS surface ensures high adhesion of platinum to the substrate with sufficient electrical conductivity, as well as good matching of the thermomechanical properties of the platinum heater with the material of the gas-sensitive layer

G. Gorokh and U. Fiadosenka are with the R&D Laboratory of Nanotechnologies, Belarusian State University of Informatics and Radioelectronics, 220013 Minsk.

I. Taratyn is with Instrumentation Engineering Faculty, Micro- and Nanotechnology Department Belarusian National Technical University, 220013 Minsk, Belarus; mnt@bntu.by (IT);

I. Serdyuk is with the Saint Petersburg State University of Information Technologies, Mechanics and Optics, pr. Kronverkskii 49, St. Petersburg, 197101, Russian Federation; serdyuk_ilya@list.ru (IS);

L. Dong and C. Yue are with Engineering Research Center of Smart Microsensors and Microsystems of MOE, School of Electronics and Information, Hangzhou Dianzi University, Hangzhou, 310018, China; donglinxi@hdu.edu.cn (LD); 02241040008@hdu.edu.cn (CY).

[25,27]. Such solutions made it possible not only to reduce fundamentally the sensors energy consumption, but also to simultaneously improve some other sensor parameters [28–33]. From the point of view of the industrial mastering feasibility of thin-film metal oxide sensors on AAS and membranes, the requirements for the performance sensors characteristics and systems are increasing. To optimize design and manufacturing solutions to achieve the best performance at minimal cost, sensor simulation and machine learning techniques are used, improving their performance, increasing their accuracy and reliability [34-36]. Sensor modeling involves creating a model that predicts the sensor's response to changes in gas concentrations and environmental conditions. This allows for more accurate calibration and a better understanding of the sensor's limitations. Machine learning algorithms analyze complex sensor data, enabling real-time calibration and anomaly detection, which traditional methods cannot achieve. As a result, gas sensors become more sensitive, respond faster, and perform better in general, making them more effective for industrial monitoring and environmental protection [37-39]. Additionally, these sensors should be capable of integration into multifunctional sensor microsystems.

In this paper, we have preliminarily optimized the design and technology for creating thin-film chemical sensors on a nanoporous AAS. Taking into account the simulation results, a series of sensors for early fire detection systems using an updated technology were manufactured, which respond to gases accompanying these processes - a certain level of hydrogen and carbon monoxide concentrations. Experimental tests of technical characteristics of prototype chemical sensors on AAO with well-known, thoroughly studied and widely used for these purposes metal oxides In_2O_3–Ga_2O_3, SnO_2–Pd and In_2O_3–SnO were carried out in order to determine further prospects for practical use and implementation in production.

II. Fabrication of Thin-Film Sensors on Anodic Alumina Substrate

A. Sensor design on anodic alumina substrate

In the design of the thin film sensor on AAS, the main thermomechanical parameters of porous AA were taken into account and the thermal conductivity features in the perpendicular and tangential directions relative to the surface were considered [16]. Based on calculations to minimize heat losses, the dimensions of the chemoresistive sensor design elements were determined. The sensor crystal is a part of the AAS measuring 1.35×1.35 mm. The heater in the form of a three-loop meander with size of 210×130 μm is located on the lower side in the central crystal region. Along the meander with a gap of 20 μm, rectangular through windows in the substrate with dimensions of 100×500 μm were located. The width of the heater conductors is 24 microns. This heater form ensures uniform heating of the crystal central part with minimal energy consumption [40]. The geometric shape and heater dimensions are shown in Fig. 1(a).

The external electrodes are placed diagonally on opposite sides of the crystal; the size of the external heater electrodes is 170×250 μm. The distance from the external electrodes to the edge of the crystal is in the range of 125-130 μm. On the crystal opposite side, in the central part, there is a measuring element in the interdigital capacitor form with a single central electrode. At the same time, in terms of external dimensions, the signal element is strictly combined with the heater (Fig. 1(b)). The platinum conductor's width is 24 microns, and the gap between the electrodes is 33 μm. Information electrodes for the sensitive layer are located above the electrodes for the heater with a gap of 50 μm, equal to the thickness of the substrate, and the external contact pads are placed mirrored relative to the external contacts for the heater. The distance between the contact pads is 1065 μm, and the size of the contact pads is 250×170 μm. Fig. 1(c) shows a combined drawing of the heater and measuring element of thin film sensor on the nanoporous AAS. Fig. 1(d) shows the cross-sectional image of the substrate with the heater and the measuring element enlarged in the callouts.

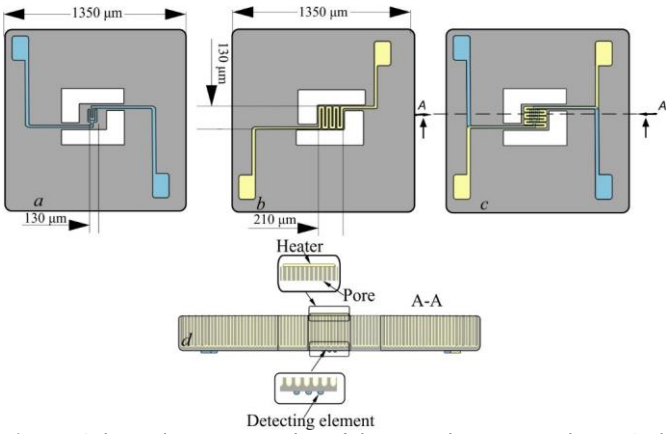

Fig. 1. Schematic representation of the crystal sensor on the AAS: (a) view of the crystal from the sensitive element side; (b) view of the crystal from the heater side; (c) combined image of the heater and detecting element; (d) the crystal image in A-A section in section with element inserts of the heater (from above) and detecting element (from above).

B. Technological route for manufacturing sensor on anodic alumina substrate

AAS were obtained by electrochemical anodization of Al foil blanks (99.99%) with dimensions of 60×48 mm^2. Before anodizing, the blanks were subjected to chemical and mechanical treatment. First, organic contaminants were removed in acetone and then micro-irregularities on the surface of the blanks were smoothed in 10% NaOH solution for 15–20 s. Then the foil was compacted, the surface was mechanically polished, and thermal straightening was carried out. After processing, the surface cleanliness of the aluminum blanks corresponded to class 12.

The prepared polished aluminum blanks were subjected to double-sided electrochemical anodization in 0.5 M oxalic acid solution to a depth of 5 μm at voltage of 50 V with a preliminary sweep of 1 V/s at temperature of 14–16 °C. The anodization rate under these conditions was 0.272 μm/min. The formed "sacrificial" AOA layer was selectively removed in a solution of orthophosphoric acid and chromic anhydride [25]. Next, one of the blanks sides was covered with a layer of chemically resistant varnish with thickness of about 15 μm and dried at room temperature for 40 minutes and in a heat chamber at 90 °C for 10 minutes. Repeated one-sided aluminum blanks anodization was carried out under the same electrochemical conditions as the first anodization. During 245 min., AA layer

with thickness of 50±1 μm was formed on the unvarnished side. Electrical anodizing modes were set using a Keysight N5752A system DC power supply; in situ recording and monitoring of process parameters was carried out using a Keysight 34470A digital multimeter connected via a USB interface to a personal computer with Bench Vue software installed.

After forming AA layer of the required thickness, the chemically resistant varnish layer was removed from the substrate, and the aluminum layer remaining after anodization was selectively etched off in solution of the following composition: $CuCl_2$ – 1.25 g/l, HCl – 1 l, distilled water 158 ml/l; at 18–22 °C for 25 min. To remove contaminants from the porous structure and adjust porosity, the formed substrate was sequentially treated in HNO_3 (90% wt.) at 18–20 °C for 1 min and in solution of H_2SO_4 (20% wt.) at 50 °C for 10 min. The porosity of AA was about 18%. The formed AAS were washed in distilled water and dried at 160 °C for 30 min. The surface morphology and cross-sections of nanoporous AAS were observed using a Hitachi S-806 scanning electron microscope at an accelerating voltage of 20 kV. Fig. 2 shows images of the surface (Fig. 2(a)), the cross section (Fig. 2(b)) and the bottom side (Fig. 2(c)) of nanoporous AAS formed according to the described technological route.

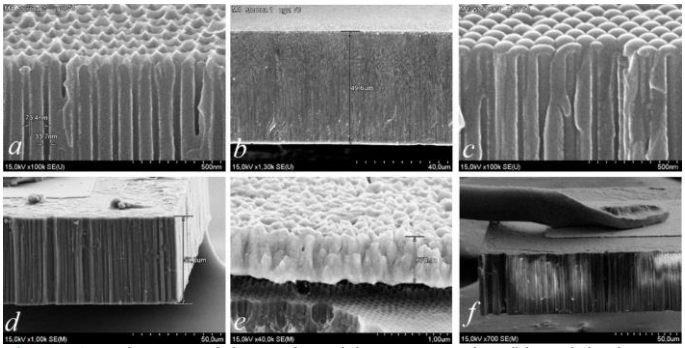

Fig. 2. SEM images of the surface (a), cross-section (b) and the bottom side of the nanoporous AAS (c); image of the sensor crystal edge with external platinum contact (d); cross-section of the gas-sensitive layer on the AAS (e); welded Pt wire on the contact pad (f).

A schematic representation of the technological route for the production of thin-film sensors on AAS is shown in Figure 3. First, platinum with thickness of 300 nm was deposited on both sides of the substrate (Fig. 3a) by magnetron deposition using an Edwards ESM100 vacuum unit with operating power W = 100 W and pressure in the working chamber $P = 5\times10^3$ mbar. Then double-sided photolithography was carried out and the heater topology was formed on one side of AAS using the method of platinum plasma-chemical etching in C_3F_8/N_2 atmosphere, and the measuring electrodes and external contact pads were formed on the reverse side (Fig. 3b). The next step was to form through holes around the heaters and separate the substrate into crystals. For this, another photolithography was performed on the pattern of through holes and separation grooves of the given size, liquid etching of AAS in H_3PO_4 (50 wt.%) at 50 °C for 5 min. and photoresist removal (Fig. 3c). At the final stage, a gas-sensitive layer (GSL) was applied to the measuring electrodes, the platinum wire was welded onto the contact pads (Fig. 3d), and the crystals were placed in the housing. Fig. 2(d–f) shows the SEM images of the crystal: d) – cross-section of crystal with contact pad; e) – fracture of gas-sensitive layer on a nanostructured substrate surface; d) – platinum wire welded to a contact pad.

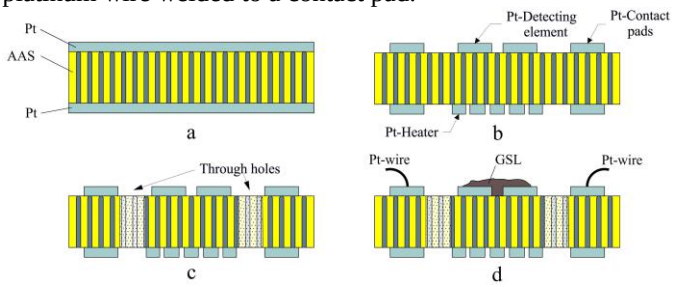

Fig. 3. Schematic representation of the technological route for the production of thin-film sensors on AAS: (a) – double-sided platinum deposition on AAS; (b) – formation of the heater, contact pads and measuring element; (c) – through holes creation and separation of the substrate into crystals; (d) – GSL application and contact pads welding.

Thin films of well-known [41] and thoroughly studied metal oxides In_2O_3–Ga_2O_3 [42,43], In_2O_3–SnO_2 [44–49] and SnO_2–Pd [50–57] were used as GSL of the chemoresistive sensors on AAS for fire detectors. To obtain indium-gallium oxide compositions, the nitrate solutions of these metals were first prepared by dissolving 10 g of $Ga(NO_3)_3$ in 20 ml of deionized water and 30 g of $In(NO_3)_3$ in 20 ml of deionized water. The solutions were mixed, and the precipitation of indium and tin hydroxides was carried out with an aqueous solution of NH_3 (30% wt.) to pH = 7.5. A colloidal solution of hydroxides, obtained after purification from electrolytes by centrifugation and chemical activation in an ultrasonic bath (2 minutes), was applied in doses of 2 μl to the surface of the measuring electrodes at 70 ºC. Each applied layer was kept at this temperature for 20 s. To obtain homogeneous gas-sensitive films of sufficient thickness (≈ 1 μm), up to 5 layers were deposited, after which the crystals were annealed in a muffle furnace at 700 °C for 40 min.

To form the gas-sensitive layer based on the oxide composition In_2O_3–SnO_2, 30 g of $In(NO_3)_3$ was initially dissolved in 20 ml of deionized water and 15 g of $SnSO_4$ in 30 ml of KOH aqueous solution (1 wt.%). The resulting solutions were mixed and the pH of the composition was adjusted to 8 by adding KOH solution (1% wt.). The preparation of the sol and its application were carried out according to the method described above. To obtain homogeneous gas-sensitive films of a given thickness (≈ 2 μm), up to 10 layers were deposited.

Tin oxide was prepared by dissolving 10 g of $SnCl_4$ in 20 ml of deionized water and adding an aqueous solution of ammonia (50% wt.) to pH=8. The resulting suspension was kept for 2 hours, and then tin hydroxide was isolated by centrifugation, washed from excess electrolytes and activated in the ultrasonic bath. Then 5 ml of $PdCl_2$ (5 wt.%) aqueous solution was added to the suspension. The colloidal solution prepared in this way was applied to the heated surface of the substrate (crystal) by dropping 2 μl. Intermediate drying of the layers was carried out at 100°C; to form the gas-sensitive SnO_2–Pd layer; the films were annealed at 700°C for 40 min.

After applying the gas-sensitive layer to the measuring element, the sensor crystal was welded using a platinum wire with a diameter of 30 μm (Fig. 2(e)) in a TO-6 housing, onto which a gas-permeable cap was placed. Fig. 4 shows the microphotograph of the sensor crystal on AAS (Fig. 4(a)), the sensor crystal welded to the external contacts of the housing

(Fig. 4(b)) and the appearance of one of the manufactured sensors intended for research tests.

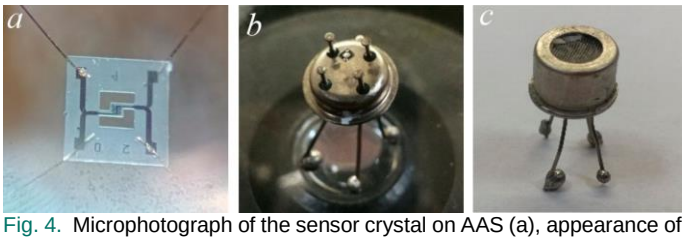

Fig. 4. Microphotograph of the sensor crystal on AAS (a), appearance of the housing welded to the external leads (b) and the prepared sensor with a cap for research tests (c).

C. Preparation of samples for research tests

Research tests of the sensors were carried out by recording low concentrations of the gases most commonly used for these purposes – hydrogen and carbon monoxide. The response of the chemical sensor to H_2 and CO was studied at power consumption values in the range of 25 to 65 mW, which ensured the heating temperature of the sensitive element in the range of 200 to 450 ºC. The study of the chemical sensor characteristics was carried out using an experimental setup consisting of a GSO PGS cylinder with the gas under study; a BKO-25-MG reducer regulating the gas flow; an EASTGAS gas mixing unit mixing the gas under study with a diluent gas (artificial air N_2–79%; O_2 – 21%); a TESTO 625 temperature and humidity meters and a flow meter for the gas mixture supplied to the chamber with the sensor. The structural image of the measuring setup is shown in Fig. 5(a). Direct measurements of the sensor parameters were carried out as part of the control and primary processing module consisting of a Keysight N5752A power supply supplying power to the heater and measuring electrodes of the sensor; a Keysight 34470A digital multimeter monitoring the supply voltage and the signal on the sensor; a temperature meter on the sensor and a normalizing amplifier. Information from the power source, readings on the multimeter, and temperature meter values were transmitted to the microcontroller, which provided collection, amplification, and transmission of the digital signal (UART – Universal Asynchronous Receiver-Transmitter) for processing on the computer and displaying the output signal on the monitor. A schematic representation of the control module and primary processing of the signal from the studied sensors is shown in Fig. 5(b).

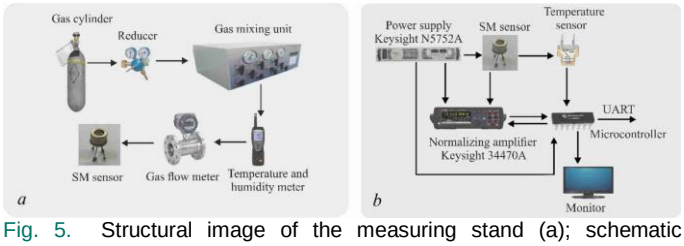

Fig. 5. Structural image of the measuring stand (a); schematic representation of the control module and the primary signal processing of the sensors under study (b).

Operational control over the progress of experiment was maintained using data recorded by measuring instruments, along with readings from a pressure gauge and flow meters of the gas generator, which were transmitted to a personal computer. The repeated measurement cycle began with turning on the gas generator valves in a combination that ensured the minimum content of the source gas in the gas mixture. After preliminary pumping, the mixture was fed into the measuring cell. On the basis of the information obtained after five measurement cycles and subsequent averaging of data recorded at the same concentrations of the gas mixture, the resistance value of the sensitive layer of the sensor was calculated.

For testing, from the manufactured batch of sensors consisting of 15 sensors, 3 series of 5 were selected, which had better stability and a quick return to the original parameters after removing the gas load.

The sensory response ($\Delta R = R_{Gas} - R_{Air}$) was defined as the difference between the sensor resistance when exposed to active gas (R_{Gas}) and the sensor resistance in air (R_{Air}) at the same heater power value. The sensitivity of the sensor was calculated as $S = R_{gas}/R_{air} \times 100\%$.

During research tests, characteristics such as reproducibility and stability of readings were recorded, as well as the effect of gas overloads on target gases and the influence of other gases and gas impurities, such as CH_4, CO_2, H_2S, NO_2, alcohol vapors, and solvents on sensor readings.

III. Research Tests of Sensors on AOA Substrate

A. Sensors with a gas-sensitive layer based on In_2O_3–Ga_2O_3

Before the tests, the current-voltage characteristics (CVC) and the dependence of the sensitive element's temperature on the dissipated power on the heater were studied. The resistance of the heaters in the sensors selected for testing was 15.6±0.8 Ohm. The tests of the sensors during heating were carried out without the gas-sensitive layer; the spread of the measurement parameters did not exceed 3%. Fig. 6(a) shows the CVC of the heater on the AOA substrate, and Fig. 6(b) shows the dependence of the temperature on the sensitive element on the dissipated power on the heater.

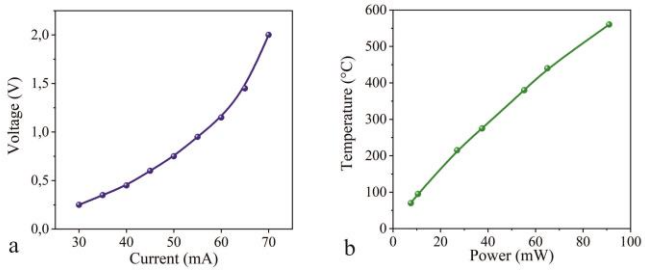

Fig. 6. Heater CVC on AAS (a), the temperature dependence at the signal electrode on the power dissipation at the heater (b).

The first batch of 5 sensors was coated with a gas-sensitive layer based on an In_2O_3–Ga_2O_3 oxide mixture. At room temperature in air, the resistance on the measuring contacts of the sensors was about 6.5 kOhm. When the heater was turned on, the resistance at 100° C was about 5 kOhm, and at 400° C it decreased to 1.5 kOhm. The resistance spread in all the studied sensors did not exceed 3–4%. Fig. 7(a) shows the temperature dependence of the In_2O_3–Ga_2O_3 gas-sensitive layer. The sensitivity of the sensors to the effects of 10 ppm H_2 and 10 ppm CO for 40–70 s was determined. Furthermore, the reproducibility of the measurement results was monitored for 15–30 min., as well as the preliminary stability for 10 days and

long-term stability for 4 months. Before each repeated measurement, a short-term annealing was performed at a current of 20 and 50 mA for 30 s.

Fig. 7(b) shows the dependence of the sensitivity of the sensors with an indium-gallium gas-sensitive layer on the time of exposure to 10 ppm H_2 at different temperatures. The maximum sensitivity of 143 % when exposed to 10 ppm H_2 for 50 s was recorded at a heater power of 23 mW, which corresponded to the heating temperature of the gas-sensitive layer of about 200° C (Fig. 7(b), curve 1). At 150 °C for 35 s, the sensitivity reached slightly more than 127 % (Fig. 7(b), curve 2), and at 120° C for 20 s, the sensitivity was only 107 %, and with further exposure to 10 ppm H_2 for 60 s it did not exceed 108 % (Fig. 7(b), curve 3). The recovery time under hydrogen exposure decreased with increasing temperature of the gas-sensitive layer and was 30, 20 and 15 s for 120° C, 150° C and 200° C, respectively.

When exposed to 10 ppm CO in the gas-sensitive layer based on the In_2O_3–Ga_2O_3 oxide mixture, the sensitivity of 167 % was achieved in 20 s at a heater power of 42 mW, which corresponded to a temperature of approximately 300 °C. The recovery time was 20 s. From the obtained dependencies it follows that the sensitivity of the sensor based on In_2O_3–Ga_2O_3 when exposed to hydrogen and carbon monoxide with a concentration of 10 ppm is decisively affected by temperature, while the reaction rate to the effect of CO and the dependence of sensitivity to CO on temperature have a pronounced character.

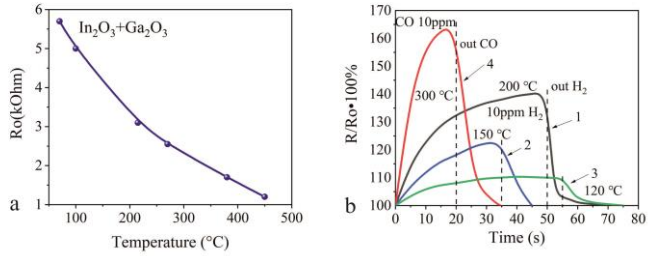

Fig. 7. Temperature dependence of the In_2O_3–Ga_2O_3 layer resistance (a); Time dependence of sensor sensitivity with In_2O_3–Ga_2O_3 gas-sensitive layer on exposure to 10 ppm H_2 at temperature of 200° C (curve 1), 150° C (curve 2), 120° C (curve 3) and on exposure to 10 ppm CO at temperature of 300° C (curve 4) (b).

TABLE I
RESISTANCE OF GCL BASED ON In_2O_3–Ga_2O_3 BEFORE AND AFTER EXPOSURE TO 10 PPM H2 AND 10 PPM CO FOR 60 S

Test period	Resistance of the GCL in air at 27 mW, kOhm	Resistance of the GCL after exposure 60s to 10 ppm H2, kOhm	Resistance of the GCL in air at 43 mW, kOhm	Resistance of the GCL after exposure 60s to 10 ppm CO, kOhm
1st day	3.64	4.81±0.45	2.42	4.19±0.54
2nd day	3.56	4.74±0.41	2.36	4.13±0.44
3rd day	3.48	4.78±0.35	2.31	4.05±0.51
4th day	3.45	4.79±0.34	2.29	4.11±0.34
5th day	3.39	4.74±0.31	2.24	4.05±0.44
8th day	3.35	4.68±0.27	2.25	4.11±0.41
9th day	3.33	4.74±0.28	2.23	4.03±0.37
10th day	3.30	4.65±0.25	2.19	4.00±0.31
1st month	3.29	4.66±0.22	2.18	4.02±0.29
2nd month	3.39	4.65±0.25	2.20	4.04±0.32
3rd month	3.29	4.63±0.25	2.21	4.01±0.24
4th month	3.28	4.64±0.24	2.21	4.04±0.26

To analyze the preliminary temporal stability, the sensor parameters were measured under the influence of 10 ppm H_2 and 10 ppm CO with continuous operation of the sensors once a day for 10 days, as well as long-term tests for 4 months, once a month. For this purpose, a supply voltage of 0.99 V was applied to the sensors, while the consumption current was 0.042 A when measuring 10 ppm CO and 0.027 A when measuring 10 ppm H_2. Before each measurement, the sensor was annealed at current of 70 mA for 1 hour at temperature of about 700° C. Table 1 shows the measured resistances of the gas-sensitive layer (GSL) in air at the measurement temperature when purging with synthetic air. The data provided are average readings obtained from different sensors during testing.

The spread of the resistances of the GCL for all the studied sensors did not exceed 3-4 %, which was a consequence of the integral technology of their manufacture, and secondly, sensors with the same characteristics were selected for the studies. Data analysis showed that the average resistance values of the GCL measured during the first 10 days decrease approximately according to a hyperbolic dependence, and in the following three months the decrease in resistance gradually fades. This nature of resistance changes without the effect of gases is preserved at different power levels in heaters of 27 mW and 43 mW. After exposure to gases, no obvious dependence of the change in resistance is observed, but during the first 10 days, the drift of the resistances of the GCL decreases from 5 % to 3 %, which stabilizes after 1-2 months of sensor operation at a level of 2-3%. This pattern is approximately the same when exposed to both 10 ppm H_2 and 10 ppm CO.

B. Sensors with the gas-sensitive layer based on SnO_2–Pd

The second batch of five sensors had GSL based on tin oxide with the addition of palladium. The annealed SnO_2–Pd film had a resistance of approximately 200 kOhm at room temperature, but when heated, its resistance decreased dramatically, and in the range of 200–300° C it was 60–30 kOhm. The Fig. 8(a) shows the temperature resistance dependence of GSL based on SnO_2–Pd, annealed at 750° C for 1 hour. During sensor measurements with tin oxide GSL with the addition of palladium nanoparticles (about 1%), high sensitivity to carbon monoxide was shown, and responses to low CO concentrations appear already at relatively low temperatures of up to 100° C. Before measurements, the sensors were pre-annealed in air by applying current of 70 mA to the heater for 5 min., and then measurements were taken at the appropriate temperature after 5 min. The effect of 5 ppm CO was carried out for 60 s, after which the chamber was blown with the purified gas for 60 s. Changes in the resistance of GSL during the effect of the measured gas were recorded with the multimeter. Fig. 8(b) shows the responses dependences of the sensors studied at different GSL temperatures. In this case, the sensor response at temperature of 80° C was already 15–17 % (Fig. 8(b), curve 1),

at temperature of 130° C – about 30 % (Fig. 8(b), curve 2), it increased with increasing temperature and at temperature of 180° C it was already 60 % (Fig. 8(b), curve 3). Increasing the temperature to 230° C resulted in only a slight increase in the sensor response to 65 % (Fig. 8(b), curve 4). Therefore, the optimal operating sensor temperature range with SnO_2–Pd GSL when exposed to carbon monoxide was 160–180° C, which corresponded to dissipated power on the heater of 23–25 mW.

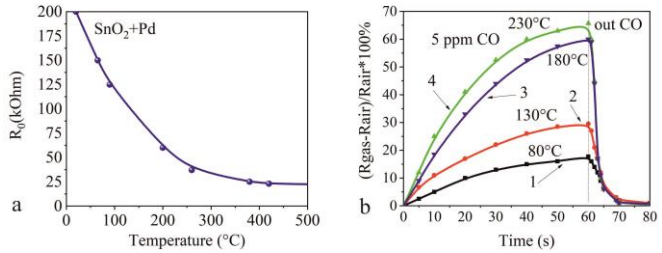

Fig. 8. Temperature dependence of the SnO_2–Pd gas-sensitive layer resistance (a); The sensory response with SnO_2–Pd gas-sensitive layer on exposure to 5 ppm CO at temperature of 80° C (curve 1), 130° C (curve 2), 180° C (curve 3) and 230° C (curve 4) (b).

Such sensors responded less dynamically to low hydrogen concentrations. Therefore, the time cycles of the sensitivity measurements had a wider range. The exposure time of 10 ppm H_2 was 120 s and, accordingly, the purging time with purified air was also 120 s. The operating temperature range was between 150° C and 180° C.

The manufactured sensors were also tested for response reproducibility (output voltage at the signal electrodes) under sequential cyclic exposure to carbon monoxide. The entire test cycle was 600 s, which included a gas exposure period of 300 s and a sensor recovery period of the next 300 s. However, initially, the sensors were tested under exposure to different carbon monoxide concentrations. Initially, after purging with purified air, the voltage at the measuring sensor electrodes was 4720 mV, when 2 ppm CO was supplied, the voltage decreased to 4510 mV. The gas supply was maintained for 15 minutes, and the voltage remained constant. Then the concentration was increased to 17 ppm, the voltage decreased to 3850 mV. After 15 minutes, the gas concentration in the chamber was again increased to 86 ppm, the voltage dropped to 2700 mV. Table 2 shows the normalized sensor readings after testing under exposure to different carbon monoxide concentrations.

TABLE II
Sensor output signal for different CO concentrations

Gas, concentration	Output voltage, mV	Signal, mV
Synthetic air	4720	-
CO, 2 ppm	4510	210
CO, 17 ppm	3850	870
CO, 86 ppm	2700	2020

After 15 minutes of sensor exposure, cyclic tests were performed by supplying 86 ppm CO for 300 s and purging the sensor with purified air for the next 300 s. The sensors showed high signal reproducibility. Fig. 9 shows the recorded voltage readings on the sensor electrodes during cyclic tests.

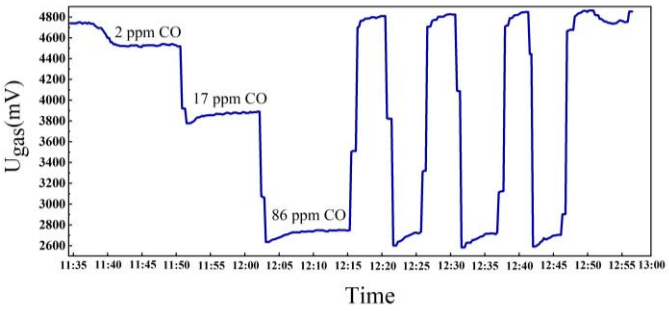

Fig. 9. Change in voltage at the measuring contacts of the sensors with SnO_2–Pd gas-sensitive layer during cyclic tests at various concentrations of gas load according to CO.

C. Sensors with the gas-sensitive layer based on In_2O_3–SnO_2.

The third batch of sensors contained the gas-sensitive layer made of the metal oxide composition In_2O_3–SnO_2. Before testing, the layer was thermally annealed at 750° C for 1 hour. After cooling, the temperature dependence of the resistance was measured, shown in Fig. 10(a). At room temperature, the resistance of In_2O_3–SnO_2 was about 70 kOhm, which decreased uniformly with increasing temperature; at about 300° C, it was 20 kOhm.

In the case of In_2O_3 and SnO_2 films obtained by the sol-gel method, layers with a low concentration of intrinsic free charge carriers are formed and, therefore, strongly respond to a change in the number of carriers as a result of adsorption of the detected gas. Fig. 10(b) shows the sensors sensitivity dependences with GSL of a mixture of semiconductor metal oxides In_2O_3–SnO_2. The highest sensitivity of the sensor with the In_2O_3–SnO_2 system to carbon monoxide was achieved at temperature of 300 °C (43 mW). When exposed to 10 ppm CO at this temperature, the sensitivity was already 250 % in 5 s, continued to grow for 30 s after gas supply and reached almost 350 % (Fig. 10(b), curve 2). In this case, layers with a low concentration of intrinsic free charge carriers are formed in films of mixture of In_2O_3 and SnO_2 oxides obtained by the sol-gel method, and they react strongly to changes in the number of carriers as a result of adsorption of the detected gas, in particular CO.

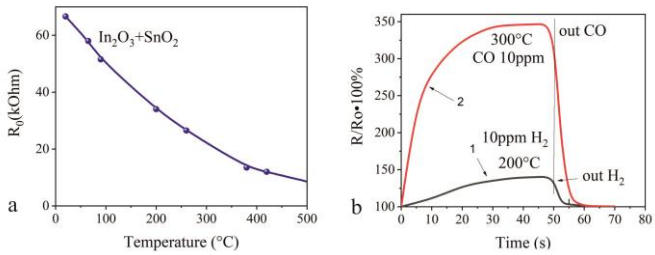

Fig. 10. Temperature dependence of the In_2O_3–SnO_2 gas-sensitive layer resistance (a); Time dependence of the sensor sensitivity with In_2O_3–SnO_2 gas-sensitive layer on exposure to 10 ppm H_2 at temperature of 200° C (curve 1), and on exposure to 10 ppm CO at temperature of 300° C (curve 2) (b).

When exposed to 10 ppm H_2 at temperature 200 ºC (22 mW), the sensor sensitivity was about 140 % (Fig. 10(b), curve 1). At the same time, the reaction of double oxides was not high. The

increasing fact in the sensitivity of In_2O_3-SnO_2 when exposed to CO and H_2 is stated in many studies [25, 33–35], but there is no clear relationship between the nature of the doping component, its concentration, the detection temperature range and the forming method of the gas-sensitive layer. In our case, the introduction of SnO_2 into the composition of In_2O_3 turned out to be very effective for recording low carbon monoxide concentrations, but did not show a noticeable effect on the sensitivity to hydrogen. Cyclic tests of sensors with In_2O_3-SnO_2 GSL showed, as in the case of In_2O_3–Ga_2O_3 metal oxides, high repeatability of measurement results and operation stability over long periods, both during continuous operation and with periodic switching on.

Table 3 shows some characteristics of sensors for measuring hydrogen and carbon monoxide, manufactured using known technologies [58-63]. In terms of sensor response, power consumption, and gas concentration, the sensors developed in this study have significant advantages.

TABLE III
The sensor characteristics of known and created in this study

GSL	Gas/conc., ppm	Resp.,%	Temp.,°C	Power cons., mW	Ref.
PdO/TiO_2	H_2/500	100	-	81	[58]
SnO_2/CdO	CO/200	68	-	150	[59]
-	H_2/50	60	400	200	[60]
-	CO/20	25	450	264	[61]
	CO/10-1000	30-100	150	100	[62]
SnO_2	H_2-CO/20-200	Up to 80	20-50	>100	[63]
In_2O_3/Ga_2O_3	H_2/10	140	200	23	This study
In_2O_3/ SnO_2	CO	350	300	43	

IV. Conclusions

The tests of chemoresistive gas sensors manufactured on nanoporous substrates of anodic alumina with gas-sensitive metal oxide layers of three compositions In_2O_3–Ga_2O_3; SnO_2–Pd and In_2O_3–SnO_2 showed generally high functional characteristics. The original design of the sensors on the anodic alumina substrate ensured rapid and uniform heating of the gas-sensitive layer with minimal heat loss and dissipation during measurements. This distinctive feature of this sensor type is its low energy consumption during measurements (no more than 30–40 mW) and high operational stability over time. The technological advantage is the integral manufacturing method of crystals from AAS, high adhesion of platinum conductors to the porous substrate, ease of preparation and application of different composition gas-cleaning layers, uniformity of films by thickness and reproducibility by composition and properties. Microelectronic technological production has ensured the reproducibility of crystal parameters and sensors as a whole. Moreover, in mass production, this will affect the cost of sensors.

The gas-sensitive characteristics studies of sensors with different gas-sensitive layers to the low concentration effects of hydrogen and carbon monoxide can be summarized as follows. The maximum sensitivity to 10 ppm CO was shown by sensors with In_2O_3–Ga_2O_3 (165 %, 300° C) and In_2O_3–SnO_2 (350 %, 300° C) gas-sensitive layers with high reaction rate (5–10 s) and recovery (up to 10 s) at power consumption of approximately 40 mW. The sensitivity to 10 ppm H_2 of these films is significantly lower. Sensors with In_2O_3–SnO_2 (145 %, 200° C) and In_2O_3–Ga_2O_3 (150 %, 200° C) gas-sensitive layers exhibited response times of 20–30 s and recovery times of up to 20 s at power consumption of about 27 mW. Stable gas responses to these gases in wide temperature range were shown by SnO_2–Pd gas-sensitive films, but with lower consumption than indium-containing gas-sensitive layers. The introduction of SnO_2 into In_2O_3 proved to be very effective in recording low carbon monoxide concentrations (up to 350 % at 300° C), but did not show a noticeable effect on the sensitivity to hydrogen (approximately 145 % at 200° C). Cyclic sensors tests with all used gas-sensitive layers showed high repeatability of measurement results and operation stability over long periods, both during continuous operation and with periodic switching on.

References

[1] Y. Deng, "Semiconducting Metal Oxides for Gas Sensing," 2019, doi: 10.1007/978-981-13-5853-1.

[2] X. Liu, S. Cheng, H. Liu, S. Hu, D. Zhang, and H. Ning, "A survey on gas sensing technology," *Sensors (Basel)*, vol. 12, no. 7, pp. 9635–9665, 2012, doi: 10.3390/s120709635.

[3] L. Liu *et al.*, "Oxygen vacancies: The origin of n-type conductivity in ZnO," *Phys. Rev. B*, vol. 93, no. 23, p. 235305, Jun. 2016, doi: 10.1103/PhysRevB.93.235305.

[4] S. E. Moon, "Semiconductor-Type MEMS Gas Sensor for Real-Time Environmental Monitoring Applications," *ETRI J*, vol. 35, no. 4, pp. 617–624, Aug. 2013, doi: 10.4218/etrij.13.1912.0008.

[5] A. A. Vasiliev *et al.*, "Alumina MEMS platform for impulse semiconductor and IR optic gas sensors," *Sensors and Actuators B: Chemical*, vol. 132, no. 1, pp. 216–223, May 2008, doi: 10.1016/j.snb.2008.01.043.

[6] G. F. Fine, L. M. Cavanagh, A. Afonja, and R. Binions, "Metal Oxide Semi-Conductor Gas Sensors in Environmental Monitoring," *Sensors*, vol. 10, no. 6, pp. 5469–5502, Jun. 2010, doi: 10.3390/s100605469.

[7] E. Comini, "Metal oxides nanowires chemical/gas sensors: recent advances," *Materials Today Advances*, vol. 7, p. 100099, Sep. 2020, doi: 10.1016/j.mtadv.2020.100099.

[8] H.-J. Kim and J.-H. Lee, "Highly sensitive and selective gas sensors using p-type oxide semiconductors: Overview," *Sensors and Actuators B: Chemical*, vol. 192, pp. 607–627, Mar. 2014, doi: 10.1016/j.snb.2013.11.005.

[9] G. Korotcenkov, "Current Trends in Nanomaterials for Metal Oxide-Based Conductometric Gas Sensors: Advantages and Limitations. Part 1: 1D and 2D Nanostructures," *Nanomaterials*, vol. 10, no. 7, p. 1392, Jul. 2020, doi: 10.3390/nano10071392.

[10] X. Y. Liu, A. Wang, T. Zhang, and C.-Y. Mou, "Catalysis by gold: New insights into the support effect," *Nano Today*, vol. 8, no. 4, pp. 403–416, Aug. 2013, doi: 10.1016/j.nantod.2013.07.005.

[11] G. Korotcenkov, "The role of morphology and crystallographic structure of metal oxides in response of conductometric-type gas sensors, G. Korotcenkov, Mater. Sci. Eng. R. 61 (2008) 1-39.," *Materials Science and Engineering R Reports*, vol. 61, pp. 1–39, May 2008, doi: 10.1016/j.mser.2008.02.001.

[12] R. Younes, S. Lakkis, Y. Alayli, and M. Sawan, "Review Of Recent Trends in Gas Sensing Technologies and their Miniaturization Potential," *Sensor Review*, vol. 34, Jan. 2014, doi: 10.1108/SR-11-2012-724.

[13] H. O. Ali, "Review of porous anodic aluminium oxide (AAO) applications for sensors, MEMS and biomedical devices," *Transactions of the IMF*, vol. 95, no. 6, pp. 290–296, Nov. 2017, doi: 10.1080/00202967.2017.1358514.

[14] G. Gorokh, A. Mozalev, D. Solovei, V. Khatko, E. Llobet, and X. Correig, "Anodic formation of low-aspect-ratio porous alumina films for metal-oxide sensor application," *Electrochimica Acta*, vol. 52, no. 4, pp. 1771–1780, Dec. 2006, doi: 10.1016/j.electacta.2006.01.081.

[15] A. Mozalev *et al.*, "MEMS-microhotplate-based hydrogen gas sensor utilizing the nanostructured porous-anodic-alumina-supported WO3 active layer," *International Journal of Hydrogen Energy*, vol. 38, pp. 8011–8021, Jun. 2013, doi: 10.1016/j.ijhydene.2013.04.063.

[16] Y. Chen, M. Li, W. Yan, X. Zhuang, K. Ng, and X. Cheng, "Sensitive and Low-Power Metal Oxide Gas Sensors with a Low-Cost Microelectromechanical Heater," *ACS Omega*, vol. 6, no. 2, pp. 1216-1222, Jan. 2021, doi: 10.1021/acsomega.0c04340.

[17] N. Tsyntsaru, B. Kavas, J. Sort, M. Urgen, and J.-P. Celis, "Mechanical and frictional behaviour of nano-porous anodised aluminium," *Materials Chemistry and Physics*, vol. 148, pp. 887–895, Dec. 2014, doi: 10.1016/j.matchemphys.2014.08.066.

[18] G. Gorokh, Y. Belahurau, H. Zakhlebayeva, I. Taratyn, and V. Khatko, "Ring gyroscope sensitive element based on nanoporous alumina," *Aircraft Engineering and Aerospace Technology*, vol. 90, pp. 00–00, Nov. 2017, doi: 10.1108/AEAT-01-2015-0026.

[19] G. Gorokh, M. I. Pashechko, J. Borc, A. Lazavenka, I. A. Kashko, and A. I. Latos, "Matrix coatings based on anodic alumina with carbon nanostructures in the pores," *Applied Surface Science*, vol. 433, Oct. 2017, doi: 10.1016/j.apsusc.2017.10.117.

[20] E. Dervishi *et al.*, "Mechanical and tribological properties of anodic Al coatings as a function of anodizing conditions," *Surface and Coatings Technology*, vol. 444, p. 128652, Jun. 2022, doi: 10.1016/j.surfcoat.2022.128652.

[21] M. Amouzadeh Tabrizi, J. Ferre-Borrull, and L. F. Marsal, "Advances in Optical Biosensors and Sensors Using Nanoporous Anodic Alumina," *Sensors (Basel)*, vol. 20, no. 18, p. 5068, Sep. 2020, doi: 10.3390/s20185068.

[22] V. Khatko *et al.*, "Evolution of Surface Morphology and Crystal Texture of WO3 Layers Sputtered onto Si-supported Nanoporous Alumina Templates," *Journal of The Electrochemical Society*, vol. 155, pp. K116–K123, Jul. 2008, doi: 10.1149/1.2918902.

[23] M. N. Rumyantseva and A. M. Gas'kov, "Chemical modification of nanocrystalline metal oxides: effect of the real structure and surface chemistry on the sensor properties," *Russ Chem Bull*, vol. 57, no. 6, pp. 1106–1125, Jun. 2008, doi: 10.1007/s11172-008-0139-z.

[24] B. Lee, I. Cho, M. Kang, D. Yang, and I. Park, "Thermally/mechanically robust anodic aluminum oxide (AAO) microheater platform for low power chemoresisitve gas sensor," *Journal of Micromechanics and Microengineering*, vol. 33, Jun. 2023, doi: 10.1088/1361-6439/ace05e.

[25] G. Gorokh *et al.*, "A Micropowered Chemoresistive Sensor Based on a Thin Alumina Nanoporous Membrane and SnxBikMoyOz Nanocomposite," *Sensors*, vol. 22, p. 3640, May 2022, doi: 10.3390/s22103640.

[26] E. A. Belahurov, V. V. Khatko, G. G. Gorokh, A. I. Zakhlebayeva, O. G. Reutskaya, and I. A. Taratyn, "Low-power gas sensor on nanostructured dielectric membrane," *J. Nano Microsyst. Tech*, vol. 6, p. 40–42, 2015.

[27] J. Han *et al.*, "MEMS-based Pt film temperature sensor on an alumina substrate," *Materials Letters*, vol. 125, pp. 224–226, Jun. 2014, doi: 10.1016/j.matlet.2014.03.170.

[28] G. Wei, P. Wang, M. Li, Z. Lin, and C. Nai, "Simulation and Optimization of a Planar-Type Micro-Hotplate with Si3N4-SiO2 Transverse Composite Dielectric Layer and Annular Heater," *Micromachines*, vol. 13, p. 601, Apr. 2022, doi: 10.3390/mi13040601.

[29] I. A. Kalinin *et al.*, "High performance microheater-based catalytic hydrogen sensors fabricated on porous anodic alumina substrates," *Sensors and Actuators B: Chemical*, vol. 404, p. 135270, Apr. 2024, doi: 10.1016/j.snb.2023.135270.

[30] T. Kumeria, A. Santos, and D. Losic, "Nanoporous Anodic Alumina Platforms: Engineered Surface Chemistry and Structure for Optical Sensing Applications," *Sensors*, vol. 14, no. 7, pp. 11878–11918, Jul. 2014, doi: 10.3390/s140711878

[31] L. Degao, X. Zhao, F. Wang, C. Ai, D. Wen, and H. Zhang, "Fabrication and characteristics of the high-sensitivity humidity sensor of anodic aluminum oxide based on silicon substrates," *International Journal of Modern Physics B*, vol. 32, p. 1850199, Jun. 2018, doi: 10.1142/S0217979218501990.

[32] S. Feng and W. Ji, "Advanced Nanoporous Anodic Alumina-Based Optical Sensors for Biomedical Applications," *Frontiers in Nanotechnology*, vol. 3, May 2021, doi: 10.3389/fnano.2021.678275.

[33] G. Gorokh *et al.*, "Spatially Ordered Matrix of Nanostructured Tin–Tungsten Oxides Nanocomposites Formed by Ionic Layer Deposition for Gas Sensing," *Sensors*, vol. 21, p. 4169, Jun. 2021, doi: 10.3390/s21124169.

[34] M. H. Shahrokh Abadi and F. Yaghouti Niyat, "COMSOL-Based Modeling and Simulation of SnO2/rGO Gas Sensor for Detection of NO2," *Scientific Reports*, vol. 8, Feb. 2018, doi: 10.1038/s41598-018-20501-2.

[35] M. Abadi, M. Gholizadeh, and A. Salehi, "Modeling and simulation of a MOSFET gas sensor with platinum gate for hydrogen gas detection," *Sensors and Actuators B-chemical - SENSOR ACTUATOR B-CHEM*, vol. 141, pp. 1–6, Aug. 2009, doi: 10.1016/j.snb.2009.06.032.

[36] M. Gheibi *et al.*, "Design of a Decision Support System to Operate a NO2 Gas Sensor Using Machine Learning, Sensitive Analysis and Conceptual Control Process Modelling," *Chemosensors*, vol. 11, p. 126, Feb. 2023, doi: 10.3390/chemosensors11020126.

[37] S. Huang *et al.*, "Machine Learning-Enabled Smart Gas Sensing Platform for Identification of Industrial Gases," *Advanced Intelligent Systems*, p. 2200016, Mar. 2022, doi: 10.1002/aisy.202200016.

[38] L. Dong *et al.*, "A Characterization of the Performance of Gas Sensor Based on Heater in Different Gas Flow Rate Environments," *IEEE Transactions on Industrial Informatics*, vol. 16, pp. 6281–6290, Jan. 2020, doi: 10.1109/TII.2019.2963683.

[39] S. Yang, G. Lei, H. Xu, Z. Lan, Z. Wang, and H. Gu, "A Review of the High-Performance Gas Sensors Using Machine Learning," in *Machine Learning for Advanced Functional Materials*, N. Joshi, V. Kushvaha, and P. Madhushri, Eds., Singapore: Springer Nature, 2023, pp. 163–198. doi: 10.1007/978-981-99-0393-1_8.

[40] G. Gorokh, I. Taratyn, V. Fedosenko, O. Reutskaya, and A. Lazavenka, "Heater Topology Influence on the Functional Characteristics of Thin-Film Gas Sensors Made by MEMS-Silicon Technology," *Chemosensors*, vol. 11, p. 443, Aug. 2023, doi: 10.3390/chemosensors11080443.

[41] G. N. Gerasimov, V. F. Gromov, O. J. Ilegbusi, and L. I. Trakhtenberg, "The mechanisms of sensory phenomena in binary metal-oxide nanocomposites," *Sensors and Actuators B: Chemical*, vol. 240, pp. 613–624, Mar. 2017, doi: 10.1016/j.snb.2016.09.007.

[42] N. Yakovlev *et al.*, "Low-resistivity gas sensors based on the In2O3-Ga2O3 mixed compounds films," *Materials Today Communications*, vol. 34, p. 105241, Dec. 2022, doi: 10.1016/j.mtcomm.2022.105241.

[43] M. S. Aleksanyan, V. M. Arakelyan, V. M. Aroutiounian, and G. E. Shahnazaryan, "Investigation of gas sensor based on In2O3:Ga2O3 film," *J. Contemp. Phys.*, vol. 46, no. 2, pp. 86–92, Apr. 2011, doi: 10.3103/S1068337211020071.

[44] G. Korotcenkov, S.-D. Han, B. Cho, and V. Brinzari, "Grain size effects in sensor response of nanostructured SnO2- and In2O3-based conductometric gas sensor, G. Korotcenkov, S.D. Han, B.K. Cho, V. Brinzari, Crit. Rev. Sol. St. Mater. Sci. 34 (1-2) (2009) 1-17.," *Critical Reviews in Solid State and Material Sciences*, vol. 34, pp. 1–17, Jan. 2009.

[45] S. Kalainathan *et al.*, "Binary and Ternary Metal Oxide Semiconductor Thin Films for Effective Gas Sensing Applications: A Comprehensive Review and Future Prospects," *Progress in Materials Science*, vol. 142, p. 101222, Dec. 2023, doi: 10.1016/j.pmatsci.2023.101222.

[46] S. M. Majhi, S. T. Navale, A. Mirzaei, H. W. Kim, and S. S. Kim, "Strategies to boost chemiresistive sensing performance of In2O3-based gas sensors: an overview," *Inorg. Chem. Front.*, vol. 10, no. 12, pp. 3428–3467, Jun. 2023, doi: 10.1039/D3QI00099K.

[47] Y. Dong *et al.*, "In2O3-SnO2 Hedgehog-Like nanostructured heterojunction for acetone detection," *Applied Surface Science*, vol. 654, p. 159543, May 2024, doi: 10.1016/j.apsusc.2024.159543.

[48] R. Malik, V. Chaudhary, M. Dahiya, S. Nehra, S. Duhan, and K. Kailasam, "A low temperature, highly sensitive and fast response toluene gas sensor based on In(III)-SnO2 loaded cubic mesoporous graphitic carbon nitride," p. 127404, Nov. 2018, doi: 10.1016/j.snb.2019.127404.

[49] N. Sui, P. Zhang, T. Zhou, and T. Zhang, "Selective ppb-level ozone gas sensor based on hierarchical branch-like In2O3 nanostructure," *Sensors and Actuators B: Chemical*, vol. 336, p. 129612, Jun. 2021, doi: 10.1016/j.snb.2021.129612.

[50] Z. Cai and S. Park, "Synthesis of Pd nanoparticle-decorated SnO2 nanowires and determination of the optimum quantity of Pd nanoparticles for highly sensitive and selective hydrogen gas sensor," *Sensors and Actuators B: Chemical*, vol. 322, p. 128651, Nov. 2020, doi: 10.1016/j.snb.2020.128651.

[51] N. J. Pineau, S. D. Keller, A. T. Güntner, and S. E. Pratsinis, "Palladium embedded in SnO2 enhances the sensitivity of flame-made chemoresistive gas sensors," *Microchim Acta*, vol. 187, no. 1, p. 96, Jan. 2020, doi: 10.1007/s00604-019-4080-7.

[52] G. Li *et al.*, "Pd nanoparticles decorated SnO2 ultrathin nanosheets for highly sensitive H2 sensor: Experimental and theoretical studies," *International Journal of Hydrogen Energy*, vol. 50, Jul. 2023, doi: 10.1016/j.ijhydene.2023.06.263.

[53] A. Staerz, T. Suzuki, U. Weimar, and N. Barsan, "SnO2: The most important base material for semiconducting metal oxide-based materials,"

in *Tin Oxide Materials*, M. O. Orlandi, Ed., in Metal Oxides. , Elsevier, 2020, pp. 345–377. doi: 10.1016/B978-0-12-815924-8.00012-8.
[54] P. Kutukov *et al.*, "Influence of mono-and bimetallic PtOx, PdOx, PtPdOx clusters on CO sensing by SnO2 based gas sensors," *Nanomaterials*, vol. 8, p. 917, Nov. 2018, doi: 10.3390/nano8110917.
[55] V. T. Duoc *et al.*, "Hydrogen gas sensor based on self-heating effect of SnO2/Pt thin film with ultralow power consumption," *International Journal of Hydrogen Energy*, vol. 61, pp. 774–782, Apr. 2024, doi: 10.1016/j.ijhydene.2024.02.180.
[56] A. Gaskov, M. Rumyantseva, and A. Marikutsa, "7 - Tin oxide nanomaterials: Active centers and gas sensor properties," in *Tin Oxide Materials*, M. O. Orlandi, Ed., in Metal Oxides, Elsevier, 2020, pp. 163–218. doi: 10.1016/B978-0-12-815924-8.00007-4.
[57] X. Meng, M. Bi, Q. Xiao, and W. Gao, "Ultrasensitive gas sensor based on Pd/SnS2/SnO2 nanocomposites for rapid detection of H2," *Sensors and Actuators B: Chemical*, vol. 359, p. 131612, May 2022, doi: 10.1016/j.snb.2022.131612.
[58] T. Thathsara, M. Shafiei, C. Harrison, and R. Hocking, "Pd- and PdO-Decorated TiO2 Nanospheres: Hydrogen Sensing Properties under Visible Light Conditions at Room Temperature," *Chemosensors*, vol. 11, no. 7, p. 409, Jul. 2023, doi: 10.3390/chemosensors11070409.
[59] A. Singh and B. Yadav, "Photo-responsive highly sensitive CO2 gas sensor based on SnO2@CdO heterostructures with DFT calculations," *Surfaces and Interfaces*, vol. 34, p. 102368, Sep. 2022, doi: 10.1016/j.surfin.2022.102368.
[60] De Lima B.s., Silva W.a.s., A. L. Ndiaye, V. R. Mastelaro, and J. Brunet, "Gas sensors data analysis system: A user-friendly interface for fast and reliable response-recovery analysis," *Chemometrics and Intelligent Laboratory Systems*, vol. 220, p. 104460, 2022, doi:10.1016/j.chemolab.2021.104460.
[61] A. Baranov, D. Spirjakin, S. Akbari, and A. Somov, "Optimization of Power Consumption for Gas Sensor Nodes: A Survey," *Sensors and Actuators, A: Physical*, vol. 233, pp. 279–289, Aug. 2015, doi: 10.1016/j.sna.2015.07.016.
[62] T. Hübert, L. Brett, V. Palmisano, and M. A. Bader, "Developments in gas sensor technology for hydrogen safety," *International Journal of Hydrogen Energy*, vol. 39, Jun. 2014, doi: 10.1016/j.ijhydene.2014.05.042.
[63] S. Dhall, B. R. Mehta, A. K. Tyagi, and K. Sood, "A Review on Environmental Gas Sensor: Materials and Technologies," *Sensors International*, vol. 2, p. 100116, Jul. 2021, doi: 10.1016/j.sintl.2021.100116.

Dr. GENNADY GOROKH is currently head of Research and Development Laboratory 4.10 "Nanotechnologies" at the Belarusian State University of Informatics and Radioelectronics. He has almost 35-years experience in the formation and characterization of nanoporous alumina formation and application of continuous and nanostructured anodic oxides in the wide-ranging fields of electronics, micro- and optoelectronics (with numerous know-how). Dr. Gennady Gorokh has authored or co-authored more than 280 publications pertaining to structure-property-performance relationships of anodic films as templates for metal/oxide nanostructure fabrication.

Dr. IGOR TARATYN Associate Professor at the Department of Micro- and Nanotechnics at the Belarusian National Technical University. Research interests: Technology of micromechanical acceleration sensors, pressure sensors, and chemical sensors based on oxide semiconductor layers, barium titanate using silicon and Al2O3 substrates. Author of over 120 publications. Has over 40 author's certificates.

Mr. U. FIADOSENKA in 2022 received a master's degree in the specialty "Nanotechnology and nanomaterials" at the Belarusian State University of Informatics and Radioelectronics (BSUIR, Belarus). At the moment, he is a PhD student at the BSUIR and Hangzhou Dianzi University (HDU, China). Research interests: synthesis and formation of nanostructures of complex composites based on nanotechnology for various types of sensors and photosensitive elements. Completed internships at NRNU MEPhI (Moscow, Russian Federation), CENIMAT-i3N (Portugal), SMMERC, Hangzhou Dianzi University (China).

Dr. ILYA SERDYUK received a PhD degree from Peter St. Petersburg Polytechnic University (SPbPU), currently works in the Department of Electrical Engineering and Electronics at the St. Petersburg National Research University of Information Technologies, Mechanics and Optics (Russian Federation). His research interests include the creation of advanced sensor microsystems and thermoelectric converters.

Dr. LINXI DONG received the Ph.D. degree in microelectronics and solid-state electronics from Zhejiang University, Hangzhou, China, in 2004. He was a Visiting Scholar with the Berkeley Sensor and Actuator Center, University of California at Berkeley, Berkeley, CA, USA, from 2015 to 2016. He is currently a Professor with the Smart Microsensors and Microsystems Engineering Research Center of Ministry of Education, College of Electronics and Information, Hangzhou Dianzi University, Hangzhou. His current research interests include industrial Internet of Things, sensor peripheral processing integrated circuit (IC) design, micro-electro-mechanical system (MEMS) sensors, and resonators, including design, modeling, and fabrication of microstructures.

Mr. Chenxi Yue is currently pursuing the phD degree with Hangzhou Dianzi University, Hangzhou, China. His research interests include the integrated circuit, sensor systems, and wearable electronics device.